

Three-dimensional Solution Structure of the Calcium Channel Antagonist ω -Agatoxin IVA: Consensus Molecular Folding of Calcium Channel Blockers

Jae Il Kim^{1*}, Shiro Konishi¹, Hideo Iwai², Toshiyuki Kohno¹
Hiroaki Gouda², Ichio Shimada², Kazuki Sato¹ and Yoji Arata^{2,3}

¹Mitsubishi Kasei Institute of Life Sciences, 11 Minamiooya Machida-shi, Tokyo 194, Japan

²Faculty of Pharmaceutical Sciences, University of Tokyo Bunkyo-ku, Tokyo 113, Japan

³Water Research Institute Senge 2-1-6, Tsukuba Ibaraki 305, Japan

The three-dimensional solution structure of ω -agatoxin IVA, which is a specific blocker of the P-type calcium channel isolated from funnel web spider venom and has a molecular mass of 5.2 kDa, was determined by two dimensional ¹H NMR spectroscopy, combined with simulated annealing calculations. On the basis of 563 experimental constraints, including 516 distance constraints obtained from the nuclear Overhauser effect, 21 torsion angle (ϕ, χ^1) constraints, and 26 constraints associated with hydrogen bonds and disulfide bonds, a total of 14 converged structures were obtained. The atomic root mean square difference for the 14 converged structures with respect to the mean coordinates is 0.42 (± 0.07) Å for the backbone atoms (N, C α , C) and 0.95 (± 0.15) Å for all heavy atoms of the central part (residues 4 to 38) constrained by four disulfide bonds. The N- and C-terminal segments (residues 1 to 3 and 39 to 48, respectively) have a disordered structure in aqueous solution. The molecular structure of ω -agatoxin IVA is composed of a short triple-stranded antiparallel β -sheet, three loops, and the disordered N- and C-terminal segments. The overall β -sheet topology is +2x, -1, which is the same as that reported for ω -conotoxin GVIA, an N-type calcium channel blocker. Irrespective of differences in the number of disulfide bonds and low primary sequence homology, these two peptide toxins show a significant structural similarity in three dimensions. The whole-cell voltage-clamp recording using rat cerebellar slices suggests that the hydrophobic C-terminal segment of ω -agatoxin IVA, which does not exist in ω -conotoxin GVIA, plays a crucial role in the blocking action of ω -agatoxin IVA on the P-type calcium channel in rat cerebellar Purkinje cells. The present study provides a molecular basis for the toxin-channel interaction, and thereby provides insight into the discrimination of different subtypes of calcium channels.

© 1995 Academic Press Limited

Keywords: calcium channel blocker; ω -agatoxin IVA; proton nuclear magnetic resonance spectroscopy; structure-activity relationships; three dimensional structure similarity

*Corresponding author

Introduction

Many peptide toxins have been used as potent pharmacological tools for studying the roles of ion channels and neurotransmitter receptors (Gray *et al.*,

1988). As the number of cloned receptors and ion channels grows, the peptide toxins have become more important as specific probes for their characterization (Adams & Olivera, 1994). The venoms of scorpion, spider, and cone snail are major sources of

Abbreviations used: ω -Aga-IVA, ω -agatoxin IVA; ω -Aga-IVB, ω -agatoxin IVB; ω -CTX-GVIA, ω -conotoxin GVIA; ESI-MS, electrospray ionization mass spectrometry; Fmoc, 9-fluorenylmethoxycarbonyl; HPLC, high performance liquid chromatography; NMR, nuclear magnetic resonance; NOE, nuclear Overhauser effect; p.p.m., parts per million; RMS, root mean square; RMSD, root-mean-square deviation; TFA, trifluoroacetic acid; DQF-COSY, double-quantum-filtered correlated spectroscopy; HOHAHA, homonuclear Hartmann-Hahn, ω -Aga-IIIa, ω -agatoxin IIIa; ACSF, artificial cerebrospinal fluid; EGTA, ethylene glycol bis (β -aminoethyl ether)-*N,N,N',N'*-tetraacetic acid; PE-COSY, primitive exclusive COSY; TPPI, time-proportional phase incrementation.

neurotoxins, and the characterization of toxin actions is currently a major focus in the field of neuroscience.

The voltage-sensitive calcium channels are classified into several subtypes, according to their electrophysiological and pharmacological properties (Tsien *et al.*, 1988). L-type calcium channels are inhibited by dihydropyridines (Rampe & Triggle, 1989), and N-type calcium channels are selectively blocked by ω -conotoxin GVIA (ω -CTX-GVIA), a 27mer peptide toxin isolated from the predatory marine snail *Conus geographus* (Olivera *et al.*, 1984; McCleskey *et al.*, 1987). The P-type calcium channels (Uchitel *et al.*, 1992) in rat Purkinje neurons are selectively blocked by ω -agatoxin IVA (ω -Aga-IVA), a 48mer peptide toxin isolated from the funnel web spider *Agelenopsis aperta* (Mintz *et al.*, 1992a,b).

The two peptide toxins ω -Aga-IVA and ω -CTX-GVIA are best characterized, in their biological actions, among many calcium channel blockers, and are the toxins most widely used for the identification of calcium channels associated with particular synaptic transmissions. Recently, the three-dimensional structure of ω -CTX-GVIA (Davis *et al.*, 1993; Pallaghy *et al.*, 1993; Sevilla *et al.*, 1993; Skalicky *et al.*, 1993) was determined using NMR spectroscopy, and its active site was revealed by the synthesis of a series of analogs with alanine substitution (Sato *et al.*, 1993; Kim *et al.*, 1994). These studies on the structure-activity relationship of ω -CTX-GVIA have provided a molecular basis for the mode of interaction, as well as toxin specificity to calcium channel subtypes.

In the present study, we chemically synthesized ω -Aga-IVA by solid-phase methodology to obtain the

toxin in an amount sufficient for NMR studies. The three-dimensional structure of synthetic ω -Aga-IVA was determined in aqueous solution by two-dimensional ^1H NMR and simulated annealing calculations. On the basis of analysis of the determined structure, it appeared that the overall folding of ω -Aga-IVA shows a significant similarity to that of ω -CTX-GVIA. The solution structure of ω -Aga-IVA is also discussed in terms of the structure-activity relationship of the ω -agatoxins, determined by electrophysiological experiments using the C-terminal truncated ω -Aga-IVA.

Results

Sequence-specific resonance assignments

Sequence-specific resonance assignments were made according to the standard method for small proteins (Wüthrich, 1986). The identification of amino acid spin systems was based on scalar coupling patterns observed in double-quantum-filtered-correlated spectroscopy (DQF-COSY) and homonuclear Hartmann-Hahn (HOHAHA) experiments, and complemented with the result of nuclear Overhauser effect spectroscopy (NOESY) measurements. The identified spin systems were ordered along the primary structure of ω -Aga-IVA through interresidue sequential NOEs observed on the NOESY spectrum. The sequential connectivities were carried out by the analysis of the $\text{C}^{\alpha}\text{H}(i)\text{-NH}(i+1)$ ($d_{\alpha\text{N}}$), $\text{C}^{\beta}\text{H}(i)\text{-NH}(i+1)$ ($d_{\beta\text{N}}$), and $\text{NH}(i)\text{-NH}(i+1)$ (d_{NN}) NOEs. Since Asp, Tyr, Trp, Ser and Asn are each present only once in the primary

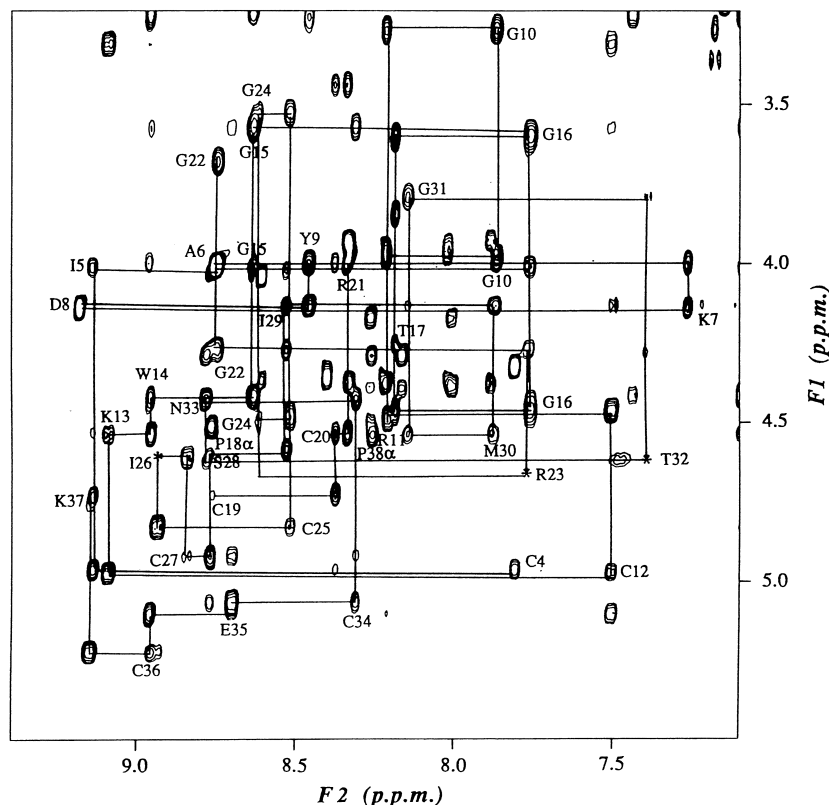


Figure 1. Sequential $d_{\alpha\text{N}}(i, i+1)$ NOE connectivities for residues 4 to 38 in the NOESY spectrum observed with a mixing time of 200 ms. The $d_{\alpha\text{N}}$ connectivities of the proline residues are shown for Pro18/Cys19 and Pro38/Arg39. Intrareidue NH- $\text{C}^{\alpha}\text{H}$ cross-peaks not shown in this plot are indicated with asterisks (*). Intrareidue NH- $\text{C}^{\alpha}\text{H}$ cross-peaks are labeled with the residue number by standard single-letter amino acid abbreviations.

Table 1. Chemical shifts of ^1H resonances of ω -Aga-IVA at 37°C and pH 2.5

Residue	Chemical shift (p.p.m.) ^a			
	NH	C $^{\alpha}$ H	C $^{\beta}$ H	Others
Lys1		4.02	1.89, 1.89	C $^{\gamma}$ H 1.43, 1.43; C $^{\delta}$ H 1.69, 1.69; C $^{\epsilon}$ H 3.00, 3.00
Lys2	8.60	4.37	1.80, 1.71	C $^{\gamma}$ H 1.44, 1.44; C $^{\delta}$ H 1.70, 1.70; C $^{\epsilon}$ H 2.98, 2.98
Lys3	8.40	4.31	1.78, 1.72	C $^{\gamma}$ H 1.45, 1.45; C $^{\delta}$ H 1.69, 1.36; C $^{\epsilon}$ H 2.97, 2.97
Cys4	7.81	4.95	3.00, 2.78	
Ile5	9.14	4.00	2.00	C $^{\gamma}$ H 1.10, 1.10; C $^{\gamma}$ M H 0.91; C $^{\delta}$ H 0.84
Ala6	8.75	3.99	1.44	
Lys7	7.25	4.13	1.71, 1.63	C $^{\gamma}$ H 1.38, 1.38; C $^{\delta}$ H 1.63, 1.63; C $^{\epsilon}$ H 3.01, 3.01
Asp8	9.18	4.12	2.66, 2.59	
Tyr9	8.46	4.00	3.21, 3.21	C2, 6H 6.99; C3, 5H 6.80
Gly10	7.86	3.95, 3.26		
Arg11	8.21	4.47	1.81, 1.81	C $^{\gamma}$ H 1.69, 1.69; C $^{\delta}$ H 3.35, 3.26; N $^{\epsilon}$ H 7.17
Cys12	7.51	4.97	3.30, 3.30	
Lys13	9.09	4.54	1.71, 1.64	C $^{\gamma}$ H 1.34, 1.31; C $^{\delta}$ H 1.63, 1.63; C $^{\epsilon}$ H 2.96, 2.96
Trp14	8.95	4.41	3.22, 3.22	N1H 9.85; C2H 7.12; C4H 7.44; C5H 7.13; C6H 7.22; C7H 7.49
Gly15	8.64	4.00, 3.55		
Gly16	7.76	4.45, 3.58		
Thr17	8.18	4.25	3.82	C $^{\gamma}$ H 1.25
Pro18		4.51	2.31, 1.96	C $^{\gamma}$ H 2.01, 1.92; C $^{\delta}$ H 3.85, 3.85
Cys19	8.76	4.72	2.84, 2.66	
Cys20	8.37	4.53	3.43, 2.50	
Arg21	8.32	3.98	1.81, 1.76	C $^{\gamma}$ H 1.63, 1.55; C $^{\delta}$ H 3.16, 3.16; N $^{\epsilon}$ H 7.14
Gly22	8.74	4.26, 3.66		
Arg23	7.77	4.66	1.67, 1.49	C $^{\gamma}$ H 1.36, 1.36; C $^{\delta}$ H 2.95, 2.78; N $^{\epsilon}$ H 7.10
Gly24	8.63	4.47, 3.53		
Cys25	8.51	4.82	3.13, 2.97	
Ile26	8.93	4.61	1.97	C $^{\gamma}$ H 1.56, 1.44; C $^{\gamma}$ M H 1.01; C $^{\delta}$ H 0.80
Cys27	8.84	4.92	2.90, 2.90	
Ser28	8.77	4.56	4.24, 4.01	
Ile29	8.52	4.10	1.96	C $^{\gamma}$ H 1.49, 1.29; C $^{\gamma}$ M H 0.98; C $^{\delta}$ H 0.92
Met30	7.88	4.53	2.23, 1.92	C $^{\gamma}$ H 2.60, 2.49
Gly31	8.14	3.77, 3.13		
Thr32	7.39	4.62	4.27	C $^{\gamma}$ H 1.06
Asn33	8.78	4.44	3.03, 2.72	N $^{\delta}$ H 7.39, 6.79
Cys34	8.31	5.06	3.58, 2.75	
Glu35	8.70	5.12	1.75, 1.75	C $^{\gamma}$ H 2.32, 2.32
Cys36	8.96	5.23	2.79, 2.72	
Lys37	9.15	4.76	1.94, 1.68	C $^{\gamma}$ H 1.34, 1.34; C $^{\delta}$ H 1.79, 1.71; C $^{\epsilon}$ H 3.06, 3.06
Pro38		4.55	2.27, 1.92	C $^{\gamma}$ H 2.11, 1.95; C $^{\delta}$ H 3.55, 3.55
Arg39	8.25	4.29	1.77, 1.77	C $^{\delta}$ H 1.67, 1.56; C $^{\epsilon}$ H 3.15, 3.15; N $^{\epsilon}$ H 7.12
Leu40	8.16	4.39	1.59, 1.59	C $^{\gamma}$ H 1.57; C $^{\delta}$ H 0.90, 0.85
Ile41	8.00	4.17	1.85	C $^{\gamma}$ H 1.45, 1.18; C $^{\gamma}$ M H 0.88; C $^{\delta}$ H 0.83
Met42	8.26	4.49	2.09, 2.01	C $^{\gamma}$ H 2.59, 2.51
Glu43	8.20	4.37	2.12, 2.00	C $^{\gamma}$ H 2.46, 2.46
Gly44	8.33	3.93, 3.93		
Leu45	8.02	4.37	1.63, 1.63	C $^{\gamma}$ H 1.60; C $^{\delta}$ H 0.90, 0.85
Gly46	8.33	3.93, 3.93		
Leu47	7.88	4.38	1.59, 1.59	C $^{\gamma}$ H 1.56; C $^{\delta}$ H 0.90, 0.85
Ala48	8.21	4.34	1.40	

^a The ^1H chemical shifts are referenced to internal sodium 3-(trimethylsilyl)propionate-2,2,3,3- $^2\text{H}_4$ (TSP).

sequence of ω -Aga-IVA, these residues were used as starting points for the sequential assignment process. Figure 1 shows the C $^{\alpha}$ H–NH fingerprint region of the NOESY spectrum containing sequential $d_{\text{NH}}(i, i + 1)$ connectivities. It was possible to distinguish inter-residue from intraresidue NOE cross-peaks in the NOESY spectrum by comparing the same region of the DQF-COSY and HOHAHA spectra.

Sequence-specific resonance assignments of the non-NH-bearing proline residues were achieved by the observation of strong sequential NOEs between C $^{\alpha}$ H(i) and C $^{\delta}$ H^{Pro}($i + 1$). The presence of these NOE cross-peaks indicates that Pro residues in ω -Aga-IVA take the *trans* configuration. The sequence-specific resonance assignments of ω -Aga-IVA are

summarized in Table 1. Figure 2 represents the sequential NOE connectivities observed in the NOESY spectrum measured with a mixing time of 200 ms, together with the slowly exchanging amide protons and the chemical shift index.

Stereospecific assignments and dihedral angle constraints

We have established the stereospecific assignments by using $^3J_{\alpha\beta}$ coupling constants combined with the intraresidual NH–C $^{\beta}$ H and C $^{\alpha}$ H–C $^{\beta}$ H NOEs observed with a mixing time of 100 ms (Hyberts *et al.*, 1987). The $^3J_{\alpha\beta}$ coupling constants were determined by observing the primitive exclusive COSY

(PE-COSY) spectrum in $^2\text{H}_2\text{O}$ solution, in which the cross-peaks gave the passive coupling between C^α and C^β protons. On the basis of the $^3J_{\alpha\beta}$ coupling constants and the intensities of intraresidual NOEs, we have established the stereospecific assignments of the prochiral β -methylene protons and the range of χ^1 side-chain torsion angles for seven residues, i.e. Cys4, Cys19, Cys20, Arg23, Cys25, Cys34, and Lys37. For t^2g^3 , g^2g^3 , and g^2t^3 conformations around the C^α - C^β bond, the χ^1 angle was constrained in the range of $-60(\pm 40)^\circ$, $60(\pm 40)^\circ$, and $180(\pm 40)^\circ$, respectively (Wagner *et al.*, 1987).

The $^3J_{\text{HN}\alpha}$ coupling constants were estimated on the DQF-COSY spectrum and converted to ϕ angle constraints according to the following rules: for $^3J_{\text{HN}\alpha} < 5.5$ Hz, and > 8 Hz, the ϕ angle was constrained to be $-65(\pm 25)^\circ$ and $-120(\pm 40)^\circ$, respectively (Pardi *et al.*, 1984). Five residues (Lys7, Asp8, Trp14, Thr17, and Cys20) with $^3J_{\text{HN}\alpha}$ less than 5.5 Hz, and nine residues (Cys12, Lys13, Arg23, Ile26, Cys27, Met30, Thr32, Glu35, and Lys37) with $^3J_{\text{HN}\alpha}$ greater than 8 Hz, were constrained by these rules.

Secondary structure

The pattern of observed NOEs was finally interpreted in secondary order structural terms for the ω -Aga-IVA molecule. The extent of the β -strands and their relative orientation in the β -sheet structure was identified according to the criteria established by Wüthrich *et al.* (1984). This was based on large $^3J_{\text{HN}\alpha}$ coupling constants, strong sequential $d_{\alpha\text{N}}$, interstrand NH-NH and NH- C^αH connectivities, and slowly exchanging amide protons that give a discrimination of the peripheral and central strands in the β -sheet. On the basis of the results of this analysis, we have identified three short β -strands consisting of residues 10 to 12, 24 to 27 and 34 to 37, which are arranged in an antiparallel fashion, and several turns, which

are described in detail later. The location and the extent of the β -strands was further confirmed by analysis of the C^αH chemical shift (Wishart *et al.*, 1992). The H^α resonances of most of the residues included in the defined β -sheet region showed downfield shifts (Figure 2).

For the N-terminal segment (residues 1 to 3) and C-terminal segment (residues 39 to 48), we were not able to observe any secondary structural constraints, and the analysis of backbone chemical shifts showed high degeneracy for these segments. In the hydrogen-deuterium exchange experiment, all cross-peaks originating from the backbone amide proton of the N- and C-terminal segments disappeared within 30 minutes, indicating a rapid exchange of the amide proton with deuterium in solution. Both the chemical shift analysis and the amide proton exchange experiment indicate that the N- and C-terminal segments in the ω -Aga-IVA molecule take the disordered structures in aqueous solution.

Structure calculations and evaluation

For calculation of the three-dimensional structure of ω -Aga-IVA, we used the NMR experimental constraints, which consisted of 542 distance constraints and 21 torsion angle constraints. Of the 542 experimental distance constraints, there are 218 intramolecular, 154 sequential ($|i-j|=1$), 41 medium-range ($|i-j|\leq 5$), and 103 long-range ($|i-j|>5$) NOE distance constraints. Fourteen distance constraints related to hydrogen bonds were added as target values of 1.7 to 2.3 Å for NH(i)-O(j) and 2.4 to 3.3 Å for N(i)-O(j) (Gouda *et al.*, 1992).

We carried out the simulated annealing calculations starting from 100 initial random structures for ω -Aga-IVA, and selected 14 final solutions that were in good agreement with the NMR experimental constraints, for which the NOE distance and torsion

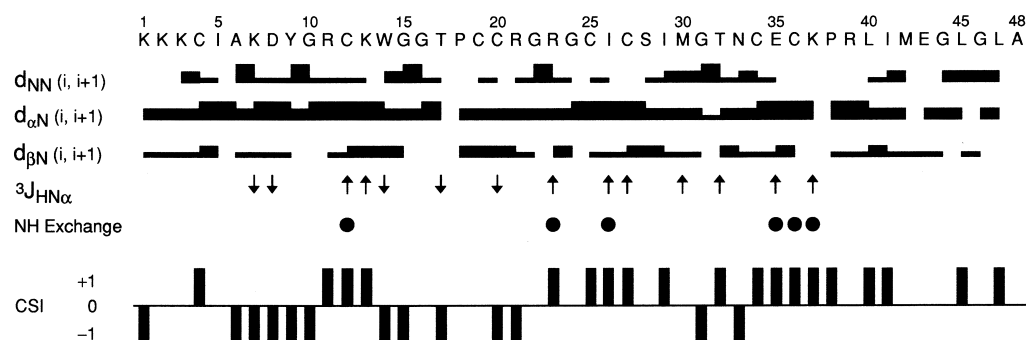


Figure 2. Summary of the sequential NOE connectivities, $^3J_{\text{HN}\alpha}$ coupling constants and slowly exchanging backbone NH protons observed in ω -Aga-IVA. These structural parameters were used for the sequence-specific assignments and the identification of secondary structure elements in ω -Aga-IVA. The sequential NOEs, d_{NN} , $d_{\alpha\text{N}}$, and $d_{\beta\text{N}}$, are indicated by bars between two residues. The NOEs are classified into strong, medium and weak, according to the height of the filled bars. The values of the $^3J_{\text{HN}\alpha}$ coupling constants are indicated by \uparrow (> 8 Hz) and \downarrow (< 5.5 Hz) symbols. Slowly exchanging backbone amide protons that are still observed in a HOHAHA spectrum recorded after 15 hours in $^2\text{H}_2\text{O}$ solution are indicated by filled circles. The chemical shift index is indicated by a ternary index with values of -1 , 0 , and $+1$. The values of -1 and $+1$ indicate a shift deviation from the random-coil value of greater than 0.1 p.p.m. upfield and downfield, respectively, and those within the range of random-coil value are indicated by 0 (Wishart *et al.*, 1992).

Table 2. Structural statistics

Structural parameter	14 converged structures ^a	Mean structure ^a
RMS deviations from experimental distance constraints (Å)		
All (542)	0.039 ± 0.001	0.037
Intraresidue (218)	0.046 ± 0.002	0.040
Sequential ($ i - j = 1$) (154)	0.047 ± 0.003	0.048
Medium range ($ i - j \leq 5$) (41)	0.008 ± 0.004	0.006
Long range ($ i - j > 5$) (103)	0.010 ± 0.002	0.014
Hydrogen bond and disulfide bond (26)	0.026 ± 0.008	0.014
RMS deviations from experimental dihedral constraints (deg.) (21)	0.169 ± 0.105	0.078
Energetic statistics (kcal mol ⁻¹) ^b		
F_{NOE}	42.6 ± 2.5	37.6
F_{tor}	0.05 ± 0.04	0.01
F_{repel}	9.18 ± 2.39	12.0
E_{L-J}	-106.5 ± 15.3	-111.1
RMS deviations from idealized geometry		
Bonds (Å)	0.003 ± 0.0001	0.003
Angles (deg.)	0.581 ± 0.013	0.595
Impropers (deg.)	0.326 ± 0.012	0.368
Average pairwise RMS differences (Å) ^c		
Backbone (N, C ^α , C)	Residues 4 to 38	Residues 10 to 12, 24 to 27, 34 to 37
All heavy atoms	0.61 ± 0.12	0.44 ± 0.11
	1.40 ± 0.21	1.25 ± 0.26

^a The 14 converged structures refer to the final set of dynamical simulated annealing structures starting from 100 initial random structures; the Mean structure was obtained by restrained minimization of the averaged coordinate of the 14 individual structures. The number of each experimental constraint used in the calculations is given in parentheses.

^b F_{NOE} , F_{tor} , and F_{repel} are the energies related to the NOE violations, the torsion angle violations, and the van der Waals repulsion term, respectively. The values of the force constants used for these terms are the standard values as depicted in the X-PLOR 3.1 manual. E_{L-J} is the Lennard-Jones van der Waals energy calculated with the CHARMM empirical energy function (Brooks *et al.*, 1983). E_{L-J} was not used in the dynamical simulated annealing calculations.

^c The RMSD values were obtained by best fitting the backbone atom coordinates for the residues 4 to 38 of the 14 individual structures. The given numbers for the backbone and all heavy atoms represent the average pairwise values ± standard deviations.

angle violations were smaller than 0.5 Å and 5°, respectively. Structural statistics for the mean and 14 converged structures were evaluated in terms of structural parameters, as shown in Table 2. The deviations from idealized covalent geometry were very small, and the Lennard-Jones van der Waals energy was large and negative, indicating that no distortions and no non-bonded bad contacts exist in the converged structures. The 14 final converged structures exhibited an atomic root-mean-square deviation (RMSD) about the mean coordinate positions for residues 4 to 38 being 0.42(±0.07) Å for the backbone atoms (N, C^α, C) and 0.95(±0.15) Å for all heavy atoms. The average pairwise RMSD between the 14 individual structures was 0.61(±0.12) Å and 1.40(±0.21) Å, respectively, for the same atom selection (Table 2). Figure 3A shows the distribution of the number of distance constraints, Figure 3B and C the atomic RMSDs, and Figure 3D and E the angular order parameters (Hyberts *et al.*, 1992) for ϕ and ψ torsion angles as a function of the residue number. Except for the N- and C-terminal segments, the structure of the backbone from Cys4 to Pro38 is well defined. The angular order parameters for most residues in this region also show high S values (>0.95), indicating that they are well defined (Figure 3D and E). However, the atomic RMSD of all heavy atoms for each of Lys7, Asp8, Arg11, Lys13, Arg21, Arg23, Met30, and Asn33 is greater than 1.1 Å (Figure 3C). These residues, except for Met30, have polar or

charged side-chains, and exist at the surface of the molecule. In a Ramachandran plot (Figure 4), the backbone dihedral angles for residues 4 to 38 of the 14 converged structures fall either in the β -sheet region or in generally allowed regions, except for those of Tyr9 and Ile29.

The N- and C-terminal segments, that were not restricted by NMR constraints, showed some apparent deviations from the sterically allowed (ϕ , ψ) limits, which reflects the randomness of the conformationally disordered backbone in these segments, as can be shown from the superposition in Figure 5A. This may result from the lack of medium and long-range NOE constraints due to inherent flexibility of both segments.

Description of the three-dimensional structure

Figure 5 shows a stereopair representation of the best-fit superposition of the backbone atoms (N, C^α, C) for the 14 converged structures. Analysis of the 14 converged structures indicates that the molecular structure of ω -Aga-IVA consists of three short β -strands, three β -turns, and the disordered N- and C-terminal segments. The three β -strands are formed by residues 10 to 12 (β -strand 1), 24 to 27 (β -strand 2), and 34 to 37 (β -strand 3).

We have identified the turns by using the standard definition that the distance between C^α(*i*) and C^α(*i* + 3) is less than 7 Å (Lewis *et al.*, 1973), and by evaluating the characteristic distance connectivities

of the backbone protons (Wüthrich, 1986), and classifying them into the types of β -turn proposed by Wilmot & Thornton (1990). The three β -turns involve residues 7 to 10 (type II), 13 to 16 (type I), and 20 to 23 (type IV, a miscellaneous type). The average dihedral angles for residues at position $i + 1$ and $i + 2$ of these β -turns are as follows: $\phi_2 = -44^\circ$, $\psi_2 = 139^\circ$ for Asp8 and $\phi_3 = 57^\circ$, $\psi_3 = 45^\circ$ for Tyr9; $\phi_2 = -67^\circ$, $\psi_2 = -12^\circ$ for Trp14 and $\phi_3 = -122^\circ$, $\psi_3 = 7^\circ$ for Gly15; $\phi_2 = -36^\circ$, $\psi_2 = -29^\circ$ for Arg21 and $\phi_3 = 121^\circ$, $\psi_3 = 31^\circ$ for Gly22. The first β -turn, as numbered from the N terminus, presents in the loop (residues 4 to 10) between β -strand 1 and the N-terminal segment.

Interestingly, a tyrosine residue (Tyr9) with a positive ϕ value is found in this β -turn. It is not common for a tyrosine residue to be found at position 3 of a type II β -turn, but this showed a $^3J_{\text{HN}\alpha}$ coupling constant of approximately 7 Hz and a very strong intraresidual NH-C α H NOE, consistent with the structural characteristics of the positive ϕ angle that was observed by NMR spectroscopy (Kline *et al.*, 1988; Ludvigsen & Poulsen, 1992). The occurrence of a positive ϕ angle for Tyr9 was also observed in ω -Aga-IVB (Yu *et al.*, 1993). The second and third β -turns present in the external long loop (residues 13 to 23) between β -strands 1 and 2. The residues (28 to

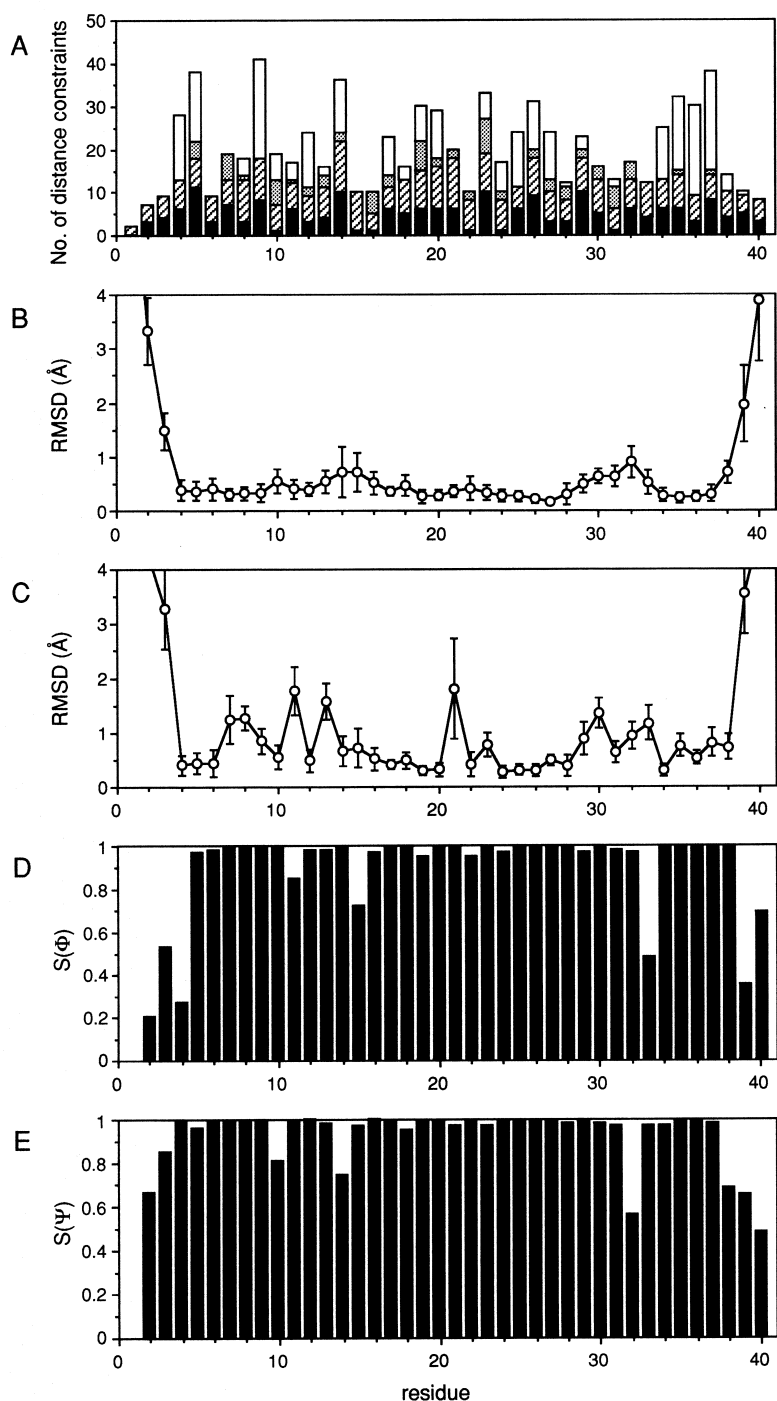


Figure 3. A, Distribution of the number of experimental distance constraints as a function of the sequence position of ω -Aga-IVA. Filled bars, intraresidue NOEs; hatched bars, sequential NOEs; stippled bars, medium-range NOEs; open bars, all long-range constraints. B and C, Distribution of the RMS difference of backbone atoms (B) and all heavy atoms (C) for the 14 converged structures about the mean structure as a function of the residue number. The bars indicate the standard deviations in these values. D and E, The angular order parameters for Φ (D) and Ψ (E) angles calculated from the 14 converged structures. The S values define the two limits of an exactly defined angle ($S = 1$) and a completely random distribution of the angle ($S = 0$).

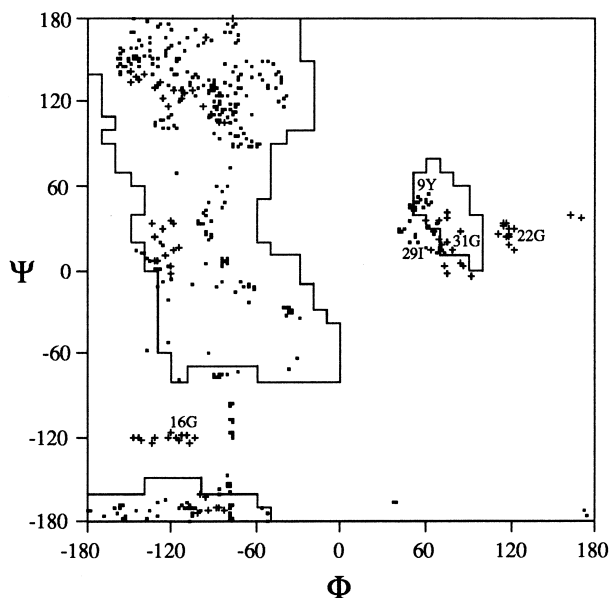


Figure 4. Ramachandran plot of the backbone conformational (Φ , Ψ) angles for the central part (residues 4 to 38) of the 14 converged structures of ω -Aga-IVA. The crosses (+) indicate glycine residues.

33) of the loop between β -strands 2 and 3 did not show the characteristic distance pattern of a tight reverse turn. In terms of RMSD, this loop was poorly defined as compared with the rest of the central part of the molecule. The angular order parameters for the peptide backbone of Trp14/Gly15 and Thr32/Asn33 show relatively low S values (Figure 3D and E), which reflects the limited number of NOE distance constraints for Gly15 and Asn33, respectively (Figure 3A).

The four disulfide bonds appear to play an important role in the formation and stabilization of the globular structure of ω -Aga-IVA. The disulfide bond between Cys12 and Cys25 interconnects β -strands 1 and 2, while the disulfide bonds between Cys4 and Cys20 and between Cys19 and Cys36 connect the external long loop with the N-terminal region and β -strand 3, respectively. The disulfide bond between Cys27 and Cys34 interconnects β -strands 2 and 3. Thus, the side-chain of Ile5 in the N-terminal region and the methyl group of Thr17 in the external long loop form a hydrophobic core of the molecule, together with the side-chains of Cys12, Cys19, Cys25 and Cys36.

Figure 5D shows the arrangement of the side-chains of the aromatic residues together with that of Ile5 in the 14 final converged structures. ω -Aga-IVA contains only two aromatic residues. The side-chain of Tyr9 is located on the bottom of the β -sheet near the end position of β -strand 3, whereas the side-chain of Trp14 is positioned on the upper side of the β -sheet in the vicinity of the starting position of the same strand. It should be noted that tyrosine and tryptophan are amphiphilic amino acids that can interact with both the hydrophilic and hydrophobic environments.

Structure-activity relationships of ω -agatoxin IVA

We synthesized a C-terminal truncated ω -Aga-IVA, and examined its biological activity in order to assess the role of the C-terminal segment in the blocking action of ω -Aga-IVA on P-type calcium channels. Using the whole-cell voltage-clamp techniques, calcium channel currents were recorded from Purkinje cells in rat cerebellar slices. Application of intact ω -Aga-IVA at a concentration of $1 \mu\text{M}$ blocked $91 \pm 2\%$ (mean \pm SEM, $n = 11$) of the high-threshold calcium channel current in Purkinje cells (Figure 6A). This is consistent with previous studies, suggesting that approximately 90% of the high-threshold calcium current is carried through the ω -Aga-IVA-sensitive P-type calcium channel (Regan, 1991; Mintz *et al.*, 1992a,b). In contrast to the potent blocking action of ω -Aga-IVA, ω -Aga-IVA (1-40) exerted only a slight, or almost no, blocking action on the P-type calcium channel current, even at the relatively high concentration of $10 \mu\text{M}$ (Figure 6B).

Based on the concentration-response relations shown in Figure 6C, it appears that ω -Aga-IVA (1-40) is at least 100-fold less potent than intact ω -Aga-IVA in the channel blocking activity. These results suggest that the C-terminal segment of ω -Aga-IVA is crucially important for its blocking action on the P-type calcium channel expressed in rat cerebellar Purkinje cells.

Discussion

In the present study, we have determined the three-dimensional structure of the calcium channel antagonist ω -Aga-IVA by ^1H NMR spectroscopy and simulated annealing calculations. The resulting solution structure shows a similar molecular folding to those of ω -Aga-IVB, which is another 48mer peptide toxin sharing nearly 70% sequence homology (Yu *et al.*, 1993), and the N-type calcium channel blocker ω -CTX-GVIA. The common structural motif of these calcium channel antagonists is comprised of three antiparallel β -strands and several reverse turns. It can be classified as having a molecular topology of $+2x, -1$ (Richardson, 1981). Recently, this topology has also been found in other, functionally unrelated, cysteine-rich polypeptide inhibitors (Pallaghy *et al.*, 1994). Below, we discuss the structure-activity relationships of the ω -agatoxins, together with the comparison of the structural characteristics between ω -Aga-IVA and ω -CTX-GVIA.

As shown in Figure 7A and B, the overall fold of ω -CTX-GVIA closely resembles the central part (residues 4 to 37) of ω -Aga-IVA, which is the most well-defined region. Despite their very low homology in the primary sequence, these two toxins share a very similar location and orientation of secondary structures in their three-dimensional structures (Figure 7C). The only conserved sequence motif can be found in the spatial arrangement of the cysteine residues in three dimensions. It is apparent

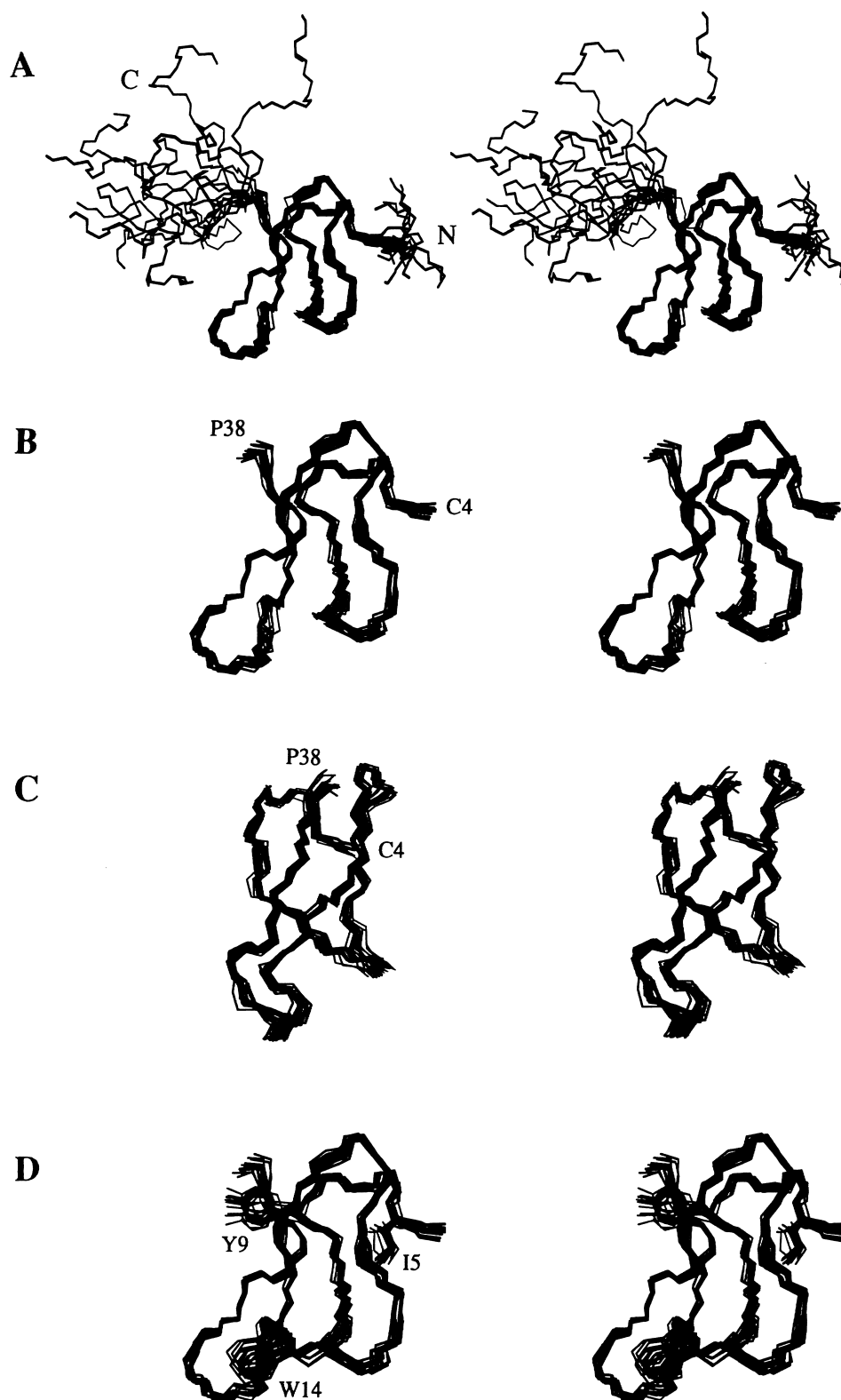


Figure 5. Stereopairs of backbone heavy atoms (N, C α , C) for the 14 converged structures of ω -Aga-IVA. These are the results of the best-fit superposition of the backbone atoms (N, C α , C, O) for the central part (residues 4 to 38) of the molecule. A, Stereopair for the complete sequence from Lys1 to Ala48. B, Stereopair for the central part (residues 4 to 38). C, Stereopair obtained by a 90° rotation about the vertical axis of stereopair B. D, Stereopair representing the orientation of the side-chain heavy atoms of Ile5, Tyr9 and Trp14, in addition to stereopair B. The atomic coordinates of the 14 converged structures and the mean structure of ω -Aga-IVA will be deposited in the Brookhaven Protein Data Bank and are available directly from the authors on request until they have been processed and released.

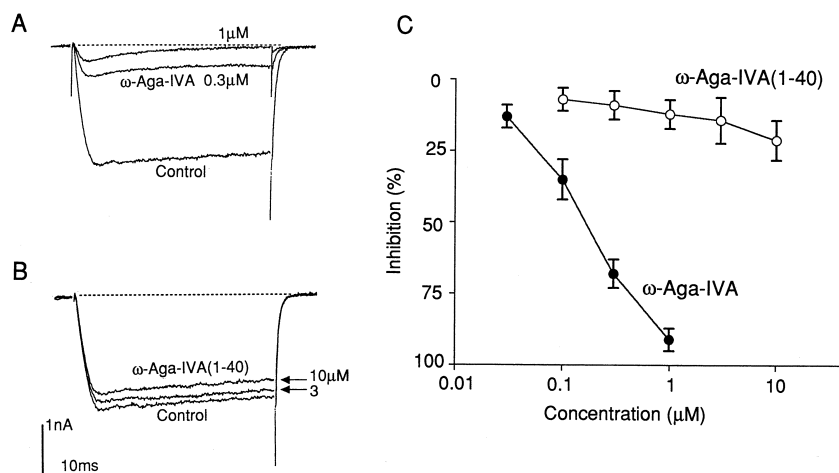


Figure 6. Effects of ω -Aga-IVA and its C-terminal truncated analog, ω -Aga-IVA (1-40), on high-threshold calcium channel currents recorded from Purkinje cells in rat cerebellar slices using the whole-cell voltage-clamp technique. A calcium current was elicited every 20 seconds by a depolarizing step from -100 to -10 mV. A and B, Currents were recorded from the same cell before and after the addition of A, Synthetic ω -Aga-IVA and B, ω -Aga-IVA (1-40). The concentrations of both peptides examined are indicated in the records. C, Concentration-response relations for synthetic ω -Aga-IVA and ω -Aga-IVA (1-40). Each point represents the mean (\pm)SEM of calcium current inhibition by each peptide determined in 3 to 15 different cells.

that three disulfide bonds between Cys4 and Cys20, between Cys12 and Cys25 and between Cys19 and Cys36 in ω -Aga-IVA correspond to those between Cys1 and Cys16, between Cys8 and Cys19 and between Cys15 and Cys26 in ω -CTX-GVIA, respectively. The disulfide bonds between Cys4 and Cys20 (ω -Aga-IVA) and between Cys1 and Cys16 (ω -CTX-GVIA) are located on the exterior of each molecule, and the remaining two disulfide bonds of each molecule are buried in the interior. An additional

disulfide bond between Cys27 and Cys34 of ω -Aga-IVA seems to contribute to the stability of the loop (residues 28 to 33) connecting the β -strands 2 and 3. In the case of ω -CTX-GVIA, the corresponding loop is formed by a hairpin turn, including two residues between Hyp21 and Lys24. Thus, it is likely that these structurally conserved disulfide connectivities significantly contribute to the maintenance of globular molecular folding of the two toxins. It can also be presumed that such a consensus of molecular

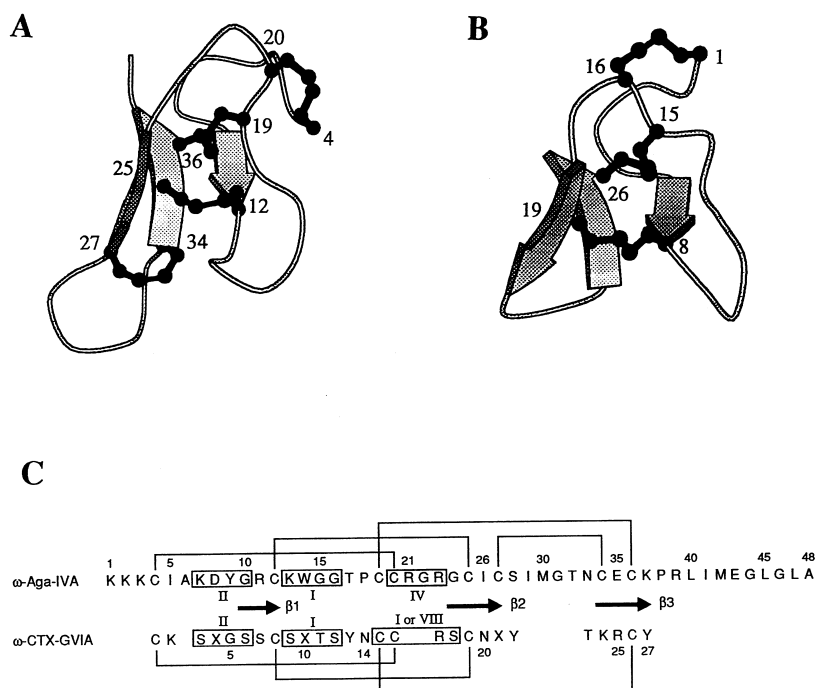


Figure 7. MOLSCRIPT (Kraulis, 1991) diagrams of the backbone peptide folding of the NMR solution structure of two calcium channel blockers. The structural topology of the triple-stranded antiparallel β -sheet is shown. A, The mean structure of ω -Aga-IVA, with four disulfide bonds between Cys4-Cys20, Cys12-Cys25, Cys19-Cys36, and Cys27-Cys34. B, The refined structure of ω -CTX-GVIA, with three disulfide bonds between Cys1-Cys16, Cys8-Cys19, and Cys15-Cys26. C, Comparative arrangements of amino acid sequences based on the distribution of secondary structure elements and disulfide bonds of ω -Aga-IVA and ω -CTX-GVIA. Hydroxyproline residues in ω -CTX-GVIA are denoted as X in single-letter amino acid abbreviations. Arrows and rectangles represent the location of β -strands and β -turns in the solution structures of the two peptide toxins, respectively. The disulfide connectivities are indicated by the horizontal lines. The ω -CTX-GVIA structure coordinates were extracted from the Brookhaven Protein Data Bank, entry ICCO (Pallaghy *et al.*, 1993).

folding is essential for the high-affinity binding of calcium channel antagonists to channel receptor sites.

Recently, it has been shown that all three calcium channel subtypes (L-, N- and P-type) can be inhibited by a single peptide toxin, designated ω -agatoxin IIIA (ω -Aga-IIIa), suggesting that ω -Aga-IIIa recognizes a binding domain common to three calcium channel subtypes (Adams & Olivera, 1994; Ertel *et al.*, 1994; Mintz, 1994). Similarly, broad subtype specificity was also observed for ω -conotoxin MVIIC (Adams & Olivera, 1994), whose sequence was deduced from a cDNA clone of the cone snail *Conus magus* (Hillyard *et al.*, 1992). These results suggest that each subtype of the calcium channel possesses a similar binding site for peptide antagonists, and seems to give a comprehensive explanation for the structural similarity between the two peptide toxins, ω -Aga-IVA and ω -CTX-GVIA.

The most significant structural difference between ω -Aga-IVA and ω -CTX-GVIA occurs in the N-terminal (residues 1 to 3) and C-terminal (residues 39 to 48) segments of ω -Aga-IVA. ω -CTX-GVIA is devoid of these segments, and those in ω -Aga-IVA take a disordered structure in aqueous solution. The N-terminal segment of ω -Aga-IVA is highly basic, whereas the C-terminal segment is highly hydrophobic. The hydrophobic nature of the C-terminal segment is also conserved in ω -Aga-IVB. It is, therefore, of interest to see whether the modification of these segments affects the toxin's blocking action on calcium channel currents. Recently, Nishio *et al.* (1993) reported that the removal of the N-terminal tripeptide did not affect the blocking action of ω -Aga-IVA on P-type calcium channels. However, little was known about the role of the C-terminal segment. In this study, we have thus examined the effects of intact ω -Aga-IVA and the C-terminal truncated ω -Aga-IVA on the calcium channel activity in Purkinje cells by electrophysiological experiments using rat cerebellar slices. The concentration-response relations for the two peptides reveal that the removal of the eight amino acids from the C terminus of ω -Aga-IVA causes a marked reduction of its activity in blocking the high-threshold calcium current in rat cerebellar Purkinje cells, which is shown to be mostly carried by the P-type calcium channel. Therefore, it is strongly suggested that the hydrophobic C-terminal region of the ω -agatoxins plays an important role in the high-affinity binding to receptor sites in the calcium channel molecule that is crucial for their blocking activity of the P-type calcium channels. The structural analysis of the C-terminal truncated ω -Aga-IVA has indicated that the loss of activity is not due to the conformational change, but to the direct interaction of the C-terminal segment with the P-type calcium channel molecules (data not shown).

Other possible determinants that confer toxin-channel interactions were suggested by comparing the overall charge distribution for the central part of the ω -agatoxins. ω -Aga-IVA has a highly basic molecular surface, with net charges of +7 under

physiological conditions, whereas ω -Aga-IVB is an electrically neutral molecule, with a net charge of zero. Despite these different properties of the molecular surface, the structures of these two ω -agatoxins exhibit a conserved four-residue patch (Asp8, Arg21, Arg23 and Arg39), clustered on one surface of the toxin molecule, in close proximity with the flexible C-terminal segment which is rich in hydrophobic residues. Since two ω -agatoxins have similar pharmacological profiles of channel blocking in the cerebellar Purkinje neurons, as well as similar structural topology, this structural characteristic could be expected to contribute to the binding of the toxin molecule to the P-type calcium channel.

Overall, we have described here in detail the three-dimensional structure of ω -Aga-IVA, in terms of a common structural topology of calcium channel blockers, and the structure-activity relationships of the ω -agatoxins. One important implication obtained from this study is that the hydrophobic C-terminal segment, and the patch of three arginine residues, could be involved in the interaction between the P-type calcium channel and the two ω -agatoxins. These determinants are not present in the primary sequence of ω -CTX-GVIA. This may explain, at least in part, how two peptide toxins, ω -Aga-IVA and ω -CTX-GVIA, recognize the different subtypes of calcium channels and inhibit the functions of individual channel proteins. These studies on structure-activity relationships, combined with three-dimensional structures, should contribute to our better understanding of the toxin blockade mechanisms, and be useful in designing synthetic antagonists or agonists with high selectivity for the different subtypes of calcium channels.

During the preparation of this manuscript, a short correspondence was published that reported the solution structure determination of ω -Aga-IVA (Reily *et al.*, 1994), and which was followed by another correspondence that discussed a structural similarity between ω -Aga-IVA and ω -CTX-GVIA (Narasimhan *et al.*, 1994). The average RMSD for their 17 converged structures was 0.97 Å for the backbone atoms and 1.41 Å for all heavy atoms of the central part (residues 4 to 36), whereas the central part (residues 4 to 38) of our 14 final solutions has an average RMSD of 0.42 and 0.95 Å, respectively. This difference in the structural convergence between their studies and ours is probably due to the total number of the experimental constraints on both interproton distance and dihedral angle. Overall, the tertiary structure of ω -Aga-IVA is similar to that reported in the present paper.

Materials and Methods

Preparation of peptide toxin

We chemically synthesized intact ω -Aga-IVA and ω -Aga-IVA (1-40) by solid-phase methodology. Solid-phase peptide synthesis was conducted on an Applied Biosystems 431A peptide synthesizer. Fmoc amino acids and other reagents used on the synthesizer were obtained from

Applied Biosystems Japan (Chiba, Japan). Fmoc-Ala- and Fmoc-Leu-*p*-oxybenzyloxybenzyl alcohol resins were obtained from Watanabe Chemical Industries Ltd. (Hiroshima, Japan). Other reagents of peptide synthesis grade were obtained from the Peptide Institute (Osaka, Japan) or Kokusan Chemical Works Ltd. (Tokyo, Japan).

Linear precursors of ω -Aga-IVA and ω -Aga-IVA (1-40) were assembled by solid-phase methodology of Fmoc chemistry, starting with Fmoc-preloaded resin, using a trityl group for the protection of the SH groups of the cysteine residues. The oxidative folding reaction was carried out by a procedure similar to that reported by Nishio *et al.* (1993). After trifluoroacetic acid (TFA) cleavage, crude linear peptides were extracted with 2 M AcOH, and diluted to a peptide concentration of 0.02 mM in the presence of reduced/oxidized glutathione (molar ratio of peptide:GSH:GSSG was 1:100:10) and 0.5 M guanidine hydrochloride. The solutions were adjusted to pH 7.8 with aqueous NH_4OH , and stirred slowly at 4°C for three days. The crude cyclized peptides were purified by successive chromatographic procedures with Sephadex G-50F and preparative HPLC. The purities of the synthetic peptides were confirmed by analytical HPLC and electrospray ionization mass spectrometry (ESI-MS) measurement.

Electrophysiological experiments

The whole-cell voltage-clamp recording was made from Purkinje cells in rat cerebellar slices as previously described (Edwards *et al.*, 1989; Mitoma *et al.*, 1994). Brains were removed from five- to eight-day-old Wistar rats under anesthesia with sodium pentobarbital. The cerebellum was sagittally sliced at a thickness of 250 μm . After incubation with oxygenated saline for more than one hour, slices were transferred to a recording chamber on the stage of a microscope, and continuously perfused with artificial cerebrospinal fluid (ACSF) of the following composition: NaCl 139 mM, KCl 3.4 mM, CaCl_2 2.5 mM, MgCl_2 1 mM, NaHCO_3 21 mM, NaH_2PO_4 0.6 mM, glucose 10 mM. The pH of the ACSF was maintained at 7.4 by gassing with 95% (v/v) O_2 -5% (v/v) CO_2 . Recordings were made at room temperature (20 to 25°C) using patch electrodes filled with an internal solution that contained Na-GTP 0.4 mM (pH 7.4), CsCH_3SO_3 150 mM, KCl 5 mM, K-ethylene glycol bis(β -aminoethyl ether)-*N,N,N',N'*-tetraacetic acid (K-EGTA) 0.1 mM, Na-Hepes 5 mM, Mg-ATP 3 mM, and had a tip resistance of 3 to 8 M Ω .

Purkinje cells were viewed under Nomarski optics with a Zeiss 40 \times water immersion objective. After achieving whole-cell recording mode, the external solution was switched to ACSF containing BaCl_2 3 to 5 mM and tetrodotoxin 1 μM . Membrane currents were recorded with a List EPC-7 patch-clamp amplifier, and digitized for transfer to computer disk for later analysis. A series resistance compensation of 60 to 85% was used. The membrane potential of Purkinje cells was held at -70 mV. High-threshold calcium channel currents were elicited by a depolarizing step to a potential of -20 to 0 mV from a pre-holding potential of -100 mV. Leak and capacitive currents were cancelled by subtraction using the P/n method (Armstrong & Bezanilla, 1974).

Synthetic ω -Aga-IVA and ω -Aga-IVA (1-40) were dissolved in the external solution supplemented with cytochrome C (1 mg/ml) to prevent binding to containers by saturation. The synthetic peptides were applied either by perfusion or pressure pulses from micropipettes to the vicinity of the recorded neurons.

NMR measurements

NMR spectra were recorded on a Bruker AMX 500 spectrometer operating at 500 MHz for the proton frequency. All two-dimensional NMR experiments, i.e. DQF-COSY (Rance *et al.*, 1983), PE-COSY (Mueller, 1987), HOHAHA (Bax & Davis, 1985), and NOESY (Jeener *et al.*, 1979; Macura *et al.*, 1981), were performed using standard pulse sequences and phase cycling. Quadrature detection in the t_1 dimension was achieved with the time-proportional phase incrementation (TPPI) method (Marion & Wüthrich, 1983).

HOHAHA spectra were recorded with mixing times of 60 ms and 80 ms. NOESY spectra were recorded with mixing times of 100 ms, 200 ms, and 300 ms. In all experiments, 512 increments of 2 K data points were recorded with 64 to 128 transients, and were zero-filled once along the t_1 dimension. In the case of the PE-COSY experiment, the acquired data were further zero-filled once along the t_2 dimension. Suppression of undesirable t_2 ridges arising from the strong solvent resonance was achieved by linear base-line correction of the F_2 cross section, prior to Fourier transformation in the t_1 dimension. The Gauss function was used for the apodization function. The solvent resonance was suppressed by selective irradiation during the relaxation delay, which was set to 1.2 seconds. A complete set of the two-dimensional spectra were recorded at 37°C and pH 2.5 (uncorrected meter readings). Slowly exchanging backbone amide protons were identified by the analysis of HOHAHA spectra recorded at time scales of 0.5 hours, 3 hours and 15 hours. The backbone amide proton resonances originating from the β -sheet region were still observed in a HOHAHA spectrum recorded after 15 hours in $^2\text{H}_2\text{O}$ solution. The resonance assignments were also made at 30°C and pH 4.5.

The ^1H chemical shifts were referenced to internal sodium 3-(trimethylsilyl)propionate-2, 2, 3, 3- $^2\text{H}_4$ (TSP). For the NMR experiments, samples were prepared by dissolving the synthetic ω -Aga-IVA in 0.4 mL of $^2\text{H}_2\text{O}$ or H_2O containing 10% (v/v) $^2\text{H}_2\text{O}$. The peptide concentration used in all NMR measurements was about 7 mM.

Distance constraints and structure calculations

Interproton distance constraints were obtained from the NOESY spectra observed with mixing times of either 100 ms or 200 ms. Quantitative determination of the cross-peak intensities was based on the counting of the exponentially spaced contour levels. Observed NOE data were classified into three distance ranges, 1.8 to 2.5 Å, 1.8 to 3.5 Å, and 1.8 to 5 Å, corresponding to strong, medium, and weak NOEs, respectively. Pseudo-atoms were used for the methyl protons or non-stereospecifically assigned methylene protons (Wüthrich *et al.*, 1983). Correcting factors for the use of pseudo-atoms were added to the distance constraints. In addition, 0.5 Å was added to the distance constraints involving methyl protons (Clore *et al.*, 1987). Twelve additional constraints were added to define the four disulfide bonds that are present in ω -Aga-IVA. The pairing of cysteines has recently been determined by the combination of amino acid analysis, gas-phase sequencing, and mass spectrometry of proteolytic fragments (Nishio *et al.*, 1993). For each disulfide bond, we used three distance constraints, $S(i)$ - $S(j)$, $S(i)$ - $\text{C}^\beta(j)$ and $S(j)$ - $\text{C}^\beta(i)$, whose target values were set to 2.02(\pm 0.02) Å, 2.99(\pm 0.5) Å and 2.99(\pm 0.5) Å, respectively (Nilges *et al.*, 1988b).

All calculations were carried out on a HP 9000/720 workstation with the X-PLOR 3.1 program (Brünger, 1993).

The three-dimensional structure was calculated on the basis of the experimentally derived distance and torsion angle constraints by using the dynamical simulated annealing protocols. We started the calculation from a template structure with randomized backbone ϕ and ψ torsion angles. For the dynamical simulated annealing, the standard forcefield parameter set (parallhdg.pro) and topology file (topallhdg.pro) in the X-PLOR 3.1 program were used. The starting structures with a random array of atoms (Nilges *et al.*, 1988a) were regularized by the dgsa.inp protocol, and the refine.inp protocol was used for final optimization of the structures obtained from the dgsa.inp protocol. NOE distance and torsion angle constraints were applied with 50 kcal mol⁻¹ Å⁻² and 200 kcal mol⁻¹ rad⁻² force constants, respectively. The mean structure was obtained by the restrained minimization of the averaged coordinate of the final converged structures. For structural comparison, the coordinates of ω -CTX-GVIA were extracted from the Brookhaven Protein Data Bank, entry ICCO (Pallaghy *et al.*, 1993).

Acknowledgements

The authors express their thanks to Dr Terutoshi Kimura for his advice in the synthesis of ω -Aga-IVA, and Dr Katsuyoshi Masuda for ESI-MS measurement of synthetic ω -Aga-IVA. Thanks are also due to Dr Tadakazu Maeda for helpful discussion of the structural calculation.

References

- Adams, M. E. & Olivera, B. M. (1994). Neurotoxins: Overview of an emerging research technology. *Trends Neurosci.* **17**, 151–155.
- Armstrong, C. M. & Bezanilla, F. (1974). Charge movement associated with the opening and closing of the activation gates of the Na channels. *J. Gen. Physiol.* **63**, 533–552.
- Bax, A. & Davis, D. G. (1985). MLEV-17-based two-dimensional homonuclear magnetization transfer spectroscopy. *J. Magn. Reson.* **65**, 355–360.
- Brooks, B. R., Brucoleri, R. E., Olafson, B. D., States, D. J., Swaminathan, S. & Karplus, M. (1983). CHARMM: a program for macromolecular energy, minimization, and dynamics calculations. *J. Comput. Chem.* **4**, 187–217.
- Brünger, A. T. (1993). X-PLOR Manual, Version 3.1. Yale University, New Haven, CT, USA.
- Clore, G. M., Gronenborn, A. M., Nilges, M. & Ryan, C. A. (1987). Three-dimensional structure of potato carboxypeptidase inhibitor in solution. A study using nuclear magnetic resonance, distance geometry, and restrained molecular dynamics. *Biochemistry*, **26**, 8012–8023.
- Davis, J. H., Bradley, E. K., Miljanich, G. P., Nadasdi, L., Ramachandran, J. & Basus, V. J. (1993). Solution structure of ω -conotoxin GVIA using 2-D NMR spectroscopy and relaxation matrix analysis. *Biochemistry*, **32**, 7396–7405.
- Edwards, F. A., Konnerth, A., Sakmann, B. & Takahashi, T. (1989). A thin slice preparation for patch clamp recordings from neurones of the mammalian central nervous system. *Pflügers Arch.* **414**, 600–612.
- Ertel, E. A., Warren, V. A., Adams, M. E., Griffin, P. R., Cohen, C. J. & Smith, M. M. (1994). Type III ω -agatoxins: a family of probes for similar binding sites on L- and N-type calcium channels. *Biochemistry*, **33**, 5098–5108.
- Gouda, H., Torigoe, H., Saito, A., Sato, M., Arata, Y. & Shimada, I. (1992). Three-dimensional solution structure of the B domain of staphylococcal protein A: comparisons of the solution and crystal structures. *Biochemistry*, **31**, 9665–9672.
- Gray, W. R., Olivera, B. M. & Cruz, L. J. (1988). Peptide toxins from venomous conus snails. *Annu. Rev. Biochem.* **57**, 665–700.
- Hillyard, D. R., Monje, V. D., Mintz, I. M., Bean, B. P., Nadasdi, L., Ramachandran, J., Miljanich, G., Azimi-Zoonooz, A., McIntosh, J. M., Cruz, L. J., Imperial, J. S. & Olivera, B. M. (1992). A new conus peptide ligand for mammalian presynaptic Ca²⁺ channels. *Neuron*, **9**, 69–77.
- Hyberts, S. G., Marki, W. & Wagner, G. (1987). Stereo-specific assignments of side-chain protons and characterization of torsion angles in eglin c. *Eur. J. Biochem.* **164**, 625–635.
- Hyberts, S. G., Goldberg, M. S., Havel, T. F. & Wagner, G. (1992). The solution structure of eglin c based on measurements of many NOEs and coupling constants and its comparison with X-ray structures. *Protein Sci.* **1**, 736–751.
- Jeener, J., Meier, B. N., Bachmann, P. & Ernst, R. R. (1979). Investigation of exchange processes by two-dimensional NMR spectroscopy. *J. Chem. Phys.* **71**, 4546–4553.
- Kim, J. I., Takahashi, M., Ogura, A., Kohno, T., Kudo, Y. & Sato, K. (1994). Hydroxyl group of Tyr¹³ is essential for the activity of ω -conotoxin GVIA, a peptide toxin for N-type calcium channel. *J. Biol. Chem.* **269**, 23876–23878.
- Kline, A. D., Braun, W. & Wüthrich, K. (1988). Determination of the complete three-dimensional structure of the α -amylase inhibitor tendamistat in aqueous solution by nuclear magnetic resonance and distance geometry. *J. Mol. Biol.* **204**, 675–724.
- Kraulis, P. J. (1991). MOLSCRIPT: a program to produce both detailed and schematic plots of protein structures. *J. Appl. Crystallog.* **24**, 946–950.
- Lewis, P. N., Momany, F. A. & Scheraga, H. A. (1973). Chain reversals in proteins. *Biochim. Biophys. Acta*, **303**, 211–229.
- Ludvigsen, S. & Poulsen, F. M. (1992). Positive ϕ -angles in proteins by nuclear magnetic resonance spectroscopy. *J. Biomol. NMR*, **2**, 227–233.
- Macura, S., Huang, Y., Suter, D. & Ernst, R. R. (1981). Two-dimensional chemical exchange and cross-relaxation spectroscopy of coupled nuclear spins. *J. Magn. Reson.* **43**, 259–281.
- Marion, D. & Wüthrich, K. (1983). Application of phase sensitive two-dimensional correlated spectroscopy (COSY) for measurements of ¹H-¹H spin-spin coupling constants in proteins. *Biochem. Biophys. Res. Commun.* **113**, 967–974.
- McCleskey, E. W., Fox, A. P., Feldman, D. H., Cruz, L. J., Olivera, B. M., Tsien, R. W. & Yoshikami, D. (1987). ω -Conotoxin: direct and persistent blockade of specific types of calcium channels in neurons but not muscle. *Proc. Natl Acad. Sci. USA*, **84**, 4327–4331.
- Mintz, I. M. (1994). Block of Ca channels in rat central neurons by the spider toxin ω -Aga-IIIa. *J. Neurosci.* **14**, 2844–2853.
- Mintz, I. M., Adams, M. E. & Bean, B. P. (1992a). P-type calcium channels in rat central and peripheral neurons. *Neuron*, **9**, 85–95.
- Mintz, I. M., Venema, V. J., Swiderek, K. M., Lee, T. D., Bean,

- B. P. & Adams, M. E. (1992b). P-type calcium channels blocked by the spider toxin ω -Aga-IVA. *Nature*, **355**, 827–829.
- Mitoma, H., Kobayashi, T., Song, S. Y. & Konishi, S. (1994). Enhancement by serotonin of GABA-mediated inhibitory synaptic currents in rat cerebellar Purkinje cells. *Neurosci. Lett.* **173**, 127–130.
- Mueller, L. (1987). P.E. COSY, a simple alternative to E. COSY. *J. Magn. Reson.* **72**, 191–196.
- Narasimhan, L., Singh, J., Humblet, C., Guruprasad, K. & Blundell, T. (1994). Snail and spider toxins share a similar tertiary structure and 'cystine motif'. *Nature Struct. Biol.* **1**, 850–852.
- Nilges, M., Clore, G. M. & Gronenborn, A. M. (1988a). Determination of three-dimensional structures of proteins from interproton distance data by dynamical simulated annealing from a random array of atoms. *FEBS Letters*, **239**, 129–136.
- Nilges, M., Gronenborn, A. M., Brünger, A. T. & Clore, G. M. (1988b). Determination of three-dimensional structures of proteins by simulated annealing with interproton distance restraints: application to crambin, potato carboxypeptidase inhibitor and barley serine proteinase inhibitor 2. *Protein Eng.* **2**, 27–38.
- Nishio, H., Yoshizawa-Kumagaya, K., Kubo, S., Chen, Y., Momiyama, A., Takahashi, T., Kimura, T. & Sakakibara, S. (1993). Synthesis of ω -agatoxin IVA and its related peptides. *Biochem. Biophys. Res. Commun.* **196**, 1447–1453.
- Olivera, B. M., McIntosh, J. M., Cruz, L. J., Luque, F. A. & Gray, W. R. (1984). Purification and sequence of a presynaptic peptide toxin from *Conus geographus* venom. *Biochemistry*, **23**, 5087–5090.
- Pallaghy, P. K., Duggan, B. M., Pennington, M. W. & Norton, R. S. (1993). Three-dimensional structure in solution of the calcium channel blocker ω -conotoxin. *J. Mol. Biol.* **234**, 405–420.
- Pallaghy, P. K., Nielsen, K. J., Craik, D. J. & Norton, R. S. (1994). A common structural motif incorporating a cystine knot and a triple-stranded β -sheet in toxic and inhibitory polypeptides. *Protein Sci.* **3**, 1833–1839.
- Pardi, A., Billeter, M. & Wüthrich, K. (1984). Calibration of the angular dependence of the amide proton– C^{α} proton coupling constants, $^3J_{\text{HN}^{\alpha}}$, in a globular protein: Use of $^3J_{\text{HN}^{\alpha}}$ for identification of helical secondary structure. *J. Mol. Biol.* **180**, 741–751.
- Rampe, D. & Triggle, D. J. (1989). 1,4-Dihydropyridine activators and antagonists: Structural and functional distinctions. *Trends Pharmacol. Sci.* **10**, 507–511.
- Rance, M., Sørensen, O. W., Bodenhausen, G., Wagner, G., Ernst, R. R. & Wüthrich, K. (1983). Improved spectral resolution in COSY ^1H NMR spectra of proteins via double quantum filtering. *Biochem. Biophys. Res. Commun.* **117**, 479–485.
- Regan, L. J. (1991). Voltage-dependent calcium currents in Purkinje cells from rat cerebellar vermis. *J. Neurosci.* **11**, 2259–2269.
- Reily, M. D., Holub, K. E., Gray, W. R., Norris, T. M. & Adams, M. E. (1994). Structure–activity relationships for P-type calcium channel-selective ω -agatoxins. *Nature Struct. Biol.* **1**, 853–856.
- Richardson, J. S. (1981). The anatomy and taxonomy of protein structure. *Advan. Protein Chem.* **34**, 167–339.
- Sato, K., Park, N. G., Kohno, T., Maeda, T., Kim, J. I., Kato, R. & Takahashi, M. (1993). Role of basic residues for the binding of ω -conotoxin GVIA to N-type calcium channels. *Biochem. Biophys. Res. Commun.* **194**, 1292–1296.
- Sevilla, P., Bruix, M., Santoro, J., Gago, F., Garcia, A. G. & Rico, M. (1993). Three-dimensional structure of ω -conotoxin GVIA determined by ^1H NMR. *Biochem. Biophys. Res. Commun.* **192**, 1238–1244.
- Skalicky, J. J., Metzler, W. J., Ciesla, D. J., Galdes, A. & Pardi, A. (1993). Solution structure of the calcium channel antagonist ω -conotoxin GVIA. *Protein Sci.* **2**, 1591–1603.
- Tsien, R. W., Lipscombe, D., Madison, D. V., Bley, K. R. & Fox, A. P. (1988). Multiple types of neuronal calcium channels and their selective modulation. *Trends Neurosci.* **11**, 431–438.
- Uchitel, O. D., Protti, D. A., Sanchez, V., Cherksey, B. D., Sugimori, M. & Llinas, R. (1992). P-type voltage-dependent calcium channel mediates presynaptic calcium influx and transmitter release in mammalian synapses. *Proc. Natl Acad. Sci. USA*, **89**, 3330–3333.
- Wagner, G., Braun, W., Havel, T.F., Schaumann, T., Go, N. & Wüthrich, K. (1987). Protein structures in solution by nuclear magnetic resonance and distance geometry. The polypeptide fold of the basic pancreatic trypsin inhibitor determined using two different algorithms, DISGEO and DISMAN. *J. Mol. Biol.* **196**, 611–639.
- Wilmot, C. M. & Thornton, J. M. (1990). β -Turns and their distortions: A proposed new nomenclature. *Protein Eng.* **3**, 479–493.
- Wishart, D. S., Sykes, B. D. & Richards, F. M. (1992). The chemical shift index: a fast and simple method for the assignment of protein secondary structure through NMR spectroscopy. *Biochemistry*, **31**, 1647–1651.
- Wüthrich, K. (1986). *NMR of Proteins and Nucleic Acids*. John Wiley, New York, USA.
- Wüthrich, K., Billeter, M. & Braun, W. (1983). Pseudo-structures for the 20 common amino acids for use in studies of protein conformations by measurements of intramolecular proton–proton distance constraints with nuclear magnetic resonance. *J. Mol. Biol.* **169**, 949–961.
- Wüthrich, K., Billeter, M. & Braun, W. (1984). Polypeptide secondary structure determination by nuclear magnetic resonance observation of short proton–proton distances. *J. Mol. Biol.* **180**, 715–740.
- Yu, H., Rosen, M. K., Saccomano, N. A., Phillips, D., Volkman, R. A. & Schreiber, S. L. (1993). Sequential assignment and structure determination of spider toxin ω -Aga-IVB. *Biochemistry*, **32**, 13123–13129.

Edited by P. E. Wright

(Received 13 January 1995; accepted 4 May 1995)